EPJ Web of Conferences **163**, 00035 (2017) DOI: 10.1051/epjconf/201716300035
*FUSION17*

# Reaction dynamics studies for the system $^{7}$Be + $^{208}$Pb at Coulomb barrier energies

*M.* Mazzocco[1,2,⋆], *A.* Boiano[3], *C.* Boiano[4], *M.* La Commara[5,3], *C.* Manea[2], *C.* Parascandolo[3], *D.* Pierroutsakou[3], *E.* Strano[1,2], *D.* Torresi[1,2], *L.* Acosta[6], *P.* Di Meo[3], *J.P.* Fernandez-Garcia[7], *T.* Glodariu[8], *J.* Grebosz[9], *A.* Guglielmetti[10,4], *G.* Marquinez-Duran[6], *I.* Martel[6], *M.* Nicoletto[2], *A.* Pakou[11], *A.M.* Sánchez-Benítez[6], *T.* Sava[8], *O.* Sgouros[11], *C.* Signorini[1,2], *F.* Soramel[1,2], *V.* Soukeras[11], and *L.* Stroe[8]

[1] *Dipartimento di Fisica e Astronomia, Università di Padova, Padova, Italy*
[2] *INFN-Sezione di Padova, Padova, Italy*
[3] *INFN-Sezione di Napoli, Napoli, Italy*
[4] *INFN-Sezione di Milano, Milano, Italy*
[5] *Dipartimento di Fisica, Università di Napoli, Napoli, Italy*
[6] *Departamento de Fisica Aplicada, Universidad de Huelva, Huelva, Spain*
[7] *INFN-LNS, Catania, Italy*
[8] *NINPE, Magurele, Romania*
[9] *IFJ-PAN, Krakow, Poland*
[10] *Dipartimento di Fisica, Università di Milano, Milano, Italy*
[11] *Department of Physics, University of Ioannina and HINP, Ioannina, Greece*

**Abstract.** The scattering process of the Radioactive Ion Beam $^{7}$Be from a $^{208}$Pb target was measured at three near-barrier energies. The quasi-elastic angular distributions were analyzed within the framework of the optical model to extract the reaction cross sections. The results are compared with those obtained for the reactions induced by the mirror projectile $^{7}$Li and by the lightest particle-stable lithium isotope $^{6}$Li on the same target. The angular distributions for the production of the two $^{7}$Be constituent clusters, namely $^{3}$He and $^{4}$He, were also measured. In agreement with what observed for the interaction of $^{7}$Be with lighter targets, the production of the heavier helium isotope resulted to be much more abundant than that of its lighter counterpart.

## 1 Introduction

The interaction of light weakly-bound nuclei at energies around the Coulomb barrier has attracted the interest of the Nuclear Physics community for the last three decades at least (see, for instance, [1–8] and references therein). Early experiments were mainly aimed at measuring the fusion process, since theoretical calculations strongly disagreed on the predictions for the fusion cross section at sub-barrier energies. Being these projectiles rather weakly-bound, they can quite easily break up into smaller fragments while approaching a target nucleus and before a complete fusion process could occur. From a theoretical point of view, depending whether the breakup channel was treated as an additional open channel or as a removed flux from the entrance channel, models predicted either the enhancement or the hindrance of the sub-barrier fusion cross section. Discrepancies between different approaches were, in some cases, as large as four orders of magnitude.

Besides very first experiments, it was soon realized that breakup related effects enhanced the total reaction cross section at sub-barrier energies and that this increase was mainly due to direct processes rather than to compound nucleus reaction mechanisms. The attention was then turned towards the investigation of direct processes and it was observed that the large production of $\alpha$ particles at sub-barrier energies in $^{6}$He- [9–11] and $^{8}$He-induced [12, 13] reactions was essentially due to the 2n-stripping process. More recently, experiments performed with the 2n-halo $^{11}$Li [14, 15] and the 1n-halo $^{11}$Be [16] indicated that direct processes also have a quite strong influence on the elastic scattering, since large deviations from the standard Rutherford cross sections were observed already at very large impact parameters. On the other side, the data collected for the system $^{8}$B + $^{58}$Ni [17, 18] suggested that the reaction cross section enhancement at sub-barrier energies could be mainly due to the fusion process, establishing a sort of different behavior between n-rich and p-rich exotic nuclei.

The relevance of direct processes, especially of transfer channels, at near-barrier energies has been recently confirmed by the detailed studies performed at the Australian National University [19–23] for reactions induced by the stable weakly-bound nuclei $^{6,7}$Li and $^{9}$Be on a quite large variety of targets, from $^{58}$Ni to $^{209}$Bi.

⋆e-mail: marco.mazzocco@pd.infn.it

In this framework, we developed a small facility, named EXOTIC [24–26], at the Laboratori Nazionali di Legnaro (LNL) of the Istituto Nazionale di Fisica Nucleare (INFN) for the In-Flight production of light Radioactive Ion Beams (RIBs). So far, secondary beams of $^{17}$F, $^{7}$Be, $^{8}$B, $^{15}$O, $^{8}$Li and $^{10,11}$C have been delivered with intensities in the range $10^3$-$10^6$ and energies in the range 2-6 AMeV. These RIBs have been employed for reaction dynamics studies at Coulomb barrier energies, for resonant scattering experiments and to investigate processes of astrophysical interest by means of the Trojan Horse Method.

In 2010 we undertook the study of $^{7}$Be-induced reactions. This projectile was selected because is a weakly-bound p-rich nucleus with a very pronounced $^{3}$He-$^{4}$He cluster configuration in its ground state. The $^{7}$Be ($S_\alpha$ = 1.586 MeV) nuclear structure is quite similar to that of its mirror nucleus $^{7}$Li ($S_\alpha$ = 2.468 MeV), whereas its binding energy is rather close to that of the lightest particle stable lithium isotope $^{6}$Li ($S_\alpha$ = 1.475 MeV). A meaningful comparison between the $^{7}$Be and $^{6,7}$Li reaction dynamics at Coulomb barrier can easily be achieved owing to the tremendous amount of data available for the reactions induced by the stable projectiles on several different targets.

In 2014 at FUSION14 conference in New Delhi (India), the preliminary results concerning the measurement of the quasi-elastic angular distribution for the system $^{7}$Be + $^{58}$Ni at 22 MeV were presented, together with the differential cross sections for the $^{3}$He and $^{4}$He inclusive production. The final evaluation was published the following year [27]. The quasi-elastic data was in remarkable agreement with an earlier measurement performed at the University of Notre Dame (Indiana, USA) [17], while the $^{4}$He production (measured for the first time) turned out to be 4-5 times larger than that for $^{3}$He. This result clearly suggested that the near-barrier reaction dynamics was not dominated by the breakup process, in such a case, in fact, similar yields for the two helium isotopes would have been observed. Unfortunately, due to small geometrical efficiency and limited beam-time availability, no coincidences between projectile fragments were recorded. Therefore quite elaborated theoretical calculations were undertaken in order to determine the possible contributions of the n-stripping, n-pickup and exclusive breakup processes to the inclusive production cross section of $^{3}$He and $^{4}$He.

After the upgrade of the facility EXOTIC [28], we could deliver more energetic secondary beams and for the $^{7}$Be RIB, in particular, it was possible to match the energy range around the barrier for the interaction with a $^{208}$Pb target. The goals of the measurement were to measure for the first time the near-barrier quasi-elastic angular distribution and, with an improved detector setup, to detect (at least) a few coincidences between projectile fragments, in order to get a deeper insight on the reaction dynamics induced by this exotic projectile.

The paper is organized as follows: Sec. 2 will describe the secondary beam production and the experimental setup employed for the measurements. Sec. 3 will present the data analysis for the evaluation of the quasi-elastic scattering angular distributions, the theoretical analysis performed to extract the total reaction cross section, the differential cross sections for the inclusive production of $^{3}$He and $^{4}$He and the status of the analysis of coincidence events between projectile fragments. Some concluding remarks will finally be given in Sec. 4.

## 2 Experiment

The experiment was performed at INFN-LNL (Italy), where the $^{7}$Be RIB was produced by means of the facility EXOTIC. A 48.8 MeV $^{7}$Li$^{+3}$ primary beam, delivered by the LNL XTU-Tandem accelerator, was impinging on a 5-cm long gas cell doubly-walled with 2.2 $\mu$m thick Havar windows. The gas pressure was about 1 bar and the target station was kept at liquid nitrogen temperature (90K). The RIB was produced through the charge exchange reaction $^{1}$H($^{7}$Li,$^{7}$Be)n ($Q_{value}$ = -1.64 MeV) and was selected by a careful tuning of the quadrupole lenses, the dipole magnet and the Wien filter of the facility EXOTIC. Before reaching the 1 mg/cm$^2$ thick $^{208}$Pb target, the $^{7}$Be beam was crossing two Parallel Plate Avalanche Counters (PPACs) employed for beam tracking and trigger generation purposes. The outcoming secondary beam energy in these conditions was 40.5 MeV with an average intensity of about 2-3 $\times$ $10^5$ pps and a 99%-purity. A second energy of 37.6 MeV was obtained by inserting in a suitable location along the beam-line between the two PPACs a 12.5 $\mu$m thick aluminum degrader. Furthermore, an additional measurement at 42.4 MeV was performed after warming up the target at room temperature and retuning all ion optical elements of the facility.

Charged particles produced by in the interaction between the RIB and the target were detected in the angular range [$\theta_{lab}$ = 55°-165°] by means of six modules of the EXPADES detector array [29, 30]. This was actually the first experiment (after the commissioning runs) performed with this setup, whose electronics was entirely developed by our collaboration. Each EXPADES module consisted of two Double Sided Silicon Strip Detectors (DSSSDs) arranged in a $\Delta$E-E$_{res}$ telescope configuration. Each DSSSD (design BB7 from Micron Semiconductor Ltd, UK) had an active area of 62.3 mm $\times$ 62.3 mm and both sides are segmented into approximately 2-mm wide strips. To contain the cost of the electronics, the signals from the strips were 2-by-2 short-circuited at the entrance of the preamplifier board. The thickness of the EXPADES inner and outer detector was 43-57 $\mu$m and 300 $\mu$m, respectively. The six modules were placed in symmetrical locations with respect to beam axis, covering the following angular ranges: $\theta_{lab}$ = ± [55°-84°], ± [96°-125°] and ± [138°-165°]. The average distance between the detectors and the central position of the target was about 115 mm. The trigger signal for the data acquisition system was provided by the "OR" of all the silicon detectors "AND" the cathode signals from both PPACs. Trigger rates of 5-10 Hz were routinely recorded during the experiment. The acquisition times were about 48 h, 24 h and 8 h for the measurements at 40.5, 37.6 and 42.4 MeV, respectively.

## 3 Data Analysis

### 3.1 Quasi-elastic scattering

Fig. 1 shows the angular distributions for the quasi-elastic scattering process in the reaction $^{7}$Be + $^{208}$Pb at three beam energies. Due to the target thickness and the energy resolution of the secondary beam, it was not possible to distinguish in the data analysis between events generated for a pure elastic scattering process and those leading to the population of the first excited state of the projectile at 0.429 MeV. Thus, hereafter we refer to these data as "quasi-elastic". To avoid large statistical fluctuations, practically unavoidable in present-day experiments involving low-intensity RIBs, each data point in Fig. 1 originates from the counting statistics collected in four adjacent vertical strips and to the weighted average between the evaluations obtained by groups of strips located at symmetrical positions with respect to the beam axis. The error bars, which include only statistical uncertainties, clearly show that the data set at the middle energy (filled circles in Fig. 1) is the most accurate one. The quasi-elastic differential cross sections decrease as both the scattering angle and the beam energy increase, since projectile and target classically get closer to each other and more nuclear reaction channels open up.

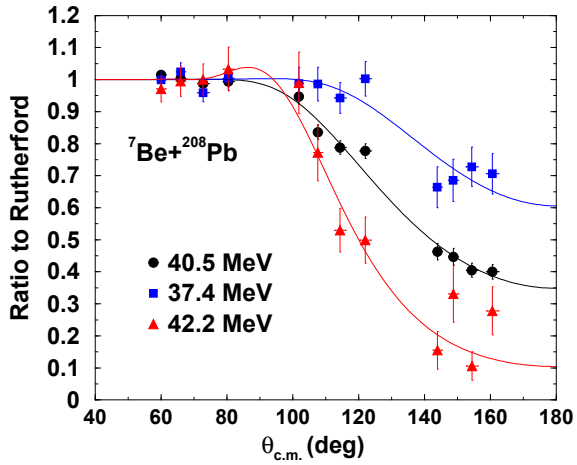


**Figure 1.** Quasi-elastic differential cross sections for the collision of the RIB $^{7}$Be with a $^{208}$Pb target at three beam energies: 40.5 MeV (circles), 37.4 MeV (squares) and 42.2 MeV (triangles). Lines are the results of a best-fit analysis of the experimental data within the framework of the optical model, as described in detail in the text.

The angular distributions plotted in Fig. 1 were analyzed within the framework of the optical model by using the code Fresco [31]. Both the real and the imaginary part of the nuclear interaction potential were described with Woods-Saxon wells. During the fitting procedure only the depths of the real ($V_0$) and imaginary ($W_0$) potential were let free to vary, whereas all other geometrical parameters were calculated according to systematics of Broglia and Winther [32] and kept fixed at the following values: $r_0 = r_i = 1.183$ fm and $a_0 = a_i = 0.63$ fm. Table 1 summarizes the results of the best-fit analysis of the experimental data and the resulting curves are plotted with continuous lines in Fig. 1.

**Table 1.** Optical model best-fit parameters of the quasi-elastic angular distributions for the reaction $^{7}$Be + $^{208}$Pb at three beam energies. The radius and diffuseness of both real and imaginary Woods-Saxon wells were fixed at the following values: $r_0 = r_i = 1.183$ fm and $a_0 = a_i = 0.63$ fm.

| E (MeV) | $V_0$ (MeV) | $W_0$ (MeV) | $\sigma_R$ (mb) | $\chi^2$ |
|---|---|---|---|---|
| 37.4 | 155.6 | 76.5 | 92.2 | 0.85 |
| 40.5 | 48.2 | 78.3 | 243.3 | 1.52 |
| 42.2 | 85.1 | 36.1 | 338.7 | 1.07 |

### 3.2 Total reaction cross section

The fourth column in Table I reports the total reaction cross sections extracted from the fitting procedure. These values are also plotted with filled circles in Fig. 2, where they are compared to the total reaction sections measured for the systems $^{6}$Li + $^{208}$Pb (diamonds) and $^{7}$Li + $^{208}$Pb (squared) [33] in a similar energy range. To make a meaningful comparison, the beam energies and the cross section values for lithium-induced reactions were normalized following the prescription given by P.R.S. Gomes *et al.* [34]. All values were than scaled to the Coulomb barrier and the geometrical size for the reaction $^{7}$Be + $^{208}$Pb.

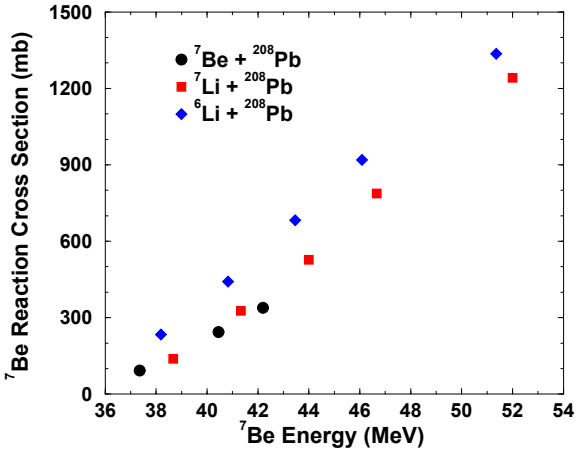


**Figure 2.** Total reaction cross sections for the systems $^{6,7}$Li + $^{208}$Pb and $^{7}$Be + $^{208}$Pb in the energy range around the Coulomb barrier. The beam energies and the cross section data for the reactions induced by lithium isotopes were scaled to account for the different Coulomb barrier and projectile geometrical size with respect to the reaction $^{7}$Be + $^{208}$Pb.

We can clearly appreciate from Fig. 2 that the $^{7}$Be data follow essentially the trend drawn by the more tightly-bound (mirror) nucleus $^{7}$Li rather than that given by the similarly weakly-bound projectile $^{6}$Li, suggesting that, for the considered nuclei, nuclear structure has a larger influence on the reaction dynamics than the binding energy. However, a clearer picture of the whole scenario can be obtained only after measuring individually the cross sections for the most relevant reaction channels, especially transfer

processes, non-capture breakup and (complete and incomplete) fusion. A first step in this direction can be done by measuring the energy spectra and the angular distributions for the inclusive production of the two $^{7}$Be constituent cluster, $^{3}$He and $^{4}$He, as described in the next paragraph.

### 3.3 $^{3}$He and $^{4}$He inclusive production

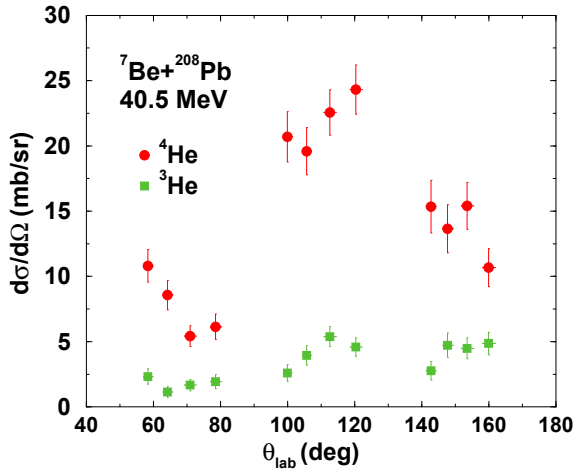


**Figure 3.** Angular distributions for the inclusive production of $^{3}$He (squared) and $^{4}$He (circles) in the reaction $^{7}$Be + $^{208}$Pb at 40.5 MeV beam energy.

Fig. 3 displays the angular distributions for the production of $^{3}$He (squared) and $^{4}$He (circles) in the interaction of the RIB $^{7}$Be with a $^{208}$Pb target at 40.5 MeV. The energy spectra for both helium isotopes evidence two distinctive components: the former mainly peaked at low-energy (2-6 MeV) with a large exponentially decreasing tail extending up to 10-12 MeV and the latter with a mostly Gaussian shape centered at about 16 and 18 MeV for $^{3}$He and $^{4}$He, respectively. The first structure should originate from particle evaporation after complete fusion reactions between beam particles and the aluminum target holder. In fact, the last collimator along the beam axis was placed too close to the second PPAC and did not prevent beam particles scattered from the PPAC exit window to hit the 60-mm wide aluminum target holder. This hypothesis is supported by three experimental evidences: (*i*) the low-energy contamination is mostly present at backward angles, being the detectors at forward angles essentially shielded by the target holder itself; (*ii*) the energy range where the maximum is located (2-6 MeV) and the exponentially decreasing behavior in the energy region up to about 12 MeV is compatible with the energy spectra of helium isotopes evaporated after a compound nucleus reaction between $^{7}$Be and $^{27}$Al [35], (*iii*) in more than 95% of coincidence events, either $^{4}$He-$^{4}$He (clear signature of n-pickup process on a $^{208}$Pb) or $^{4}$He-$^{3}$He (non capture breakup) or $^{4}$He-$^{2}$H (p-stripping), the energy of the less energetic helium fragment is larger than 12 MeV. Therefore the angular distributions plotted in Fig. 3 were obtained considering only helium isotopes whose total energy deposit was at least 12 MeV, thus minimizing possible contributions from the low-energy contamination.

Fig. 3 also illustrates that the $^{4}$He production is more abundant by a factor 4-5 with respect to probability of producing the lighter helium isotope. This outcome qualitatively agrees with what we had previously observed for the reaction induced by the same RIB on a $^{58}$Ni target. We can thus immediately conclude that, at near-barrier energies, the $^{7}$Be reaction dynamics is not dominated by the breakup process even for the interaction with a heavy target. The $^{4}$He angular distribution exhibits a maximum in the region around $\theta_{lab}$ = 120°, while that for $^{3}$He has a flatter behavior with a much less pronounced peak approximately in the same angular range. A detailed analysis of the $^{3,4}$He angular distributions and energy spectra will be the subject of a forthcoming investigation, maybe in the framework of the model recently developed by Lei and Moro [36].

### 3.4 Detection of coincidence events

As already anticipated, a few coincidence events between projectile fragments were detected at 40.5 MeV. In particular, we observed: 13 $^{4}$He-$^{2}$H (originated from the p-stripping reaction: $^{7}$Be + $^{208}$Pb → $^{6}$Li + $^{209}$Bi, $Q_{value}$ = -1.81 MeV), 19 $^{4}$He-$^{3}$He (non capture breakup, $S_{\alpha}$ = 1.586 MeV) and 17 $^{4}$He-$^{4}$He (n-pickup: $^{7}$Be + $^{208}$Pb → $^{8}$Be + $^{207}$Pb, $Q_{value}$ = +11.53 MeV) coincidence events.

Detailed kinematic calculations are presently being performed with the code Kookaburra [21] in order to derive the geometrical efficiency of the coincidence detection system and to compare theoretical predictions with the relative energy spectra, $Q_{value}$ distributions, opening and orientation angles reconstructed from the experimental data. The procedure will essentially follow the scheme described in Refs. [22, 23] and already successfully employed for the reactions: $^{6,7}$Li + $^{58}$Ni, $^{64}$Zn, $^{208}$Pb and $^{209}$Bi and $^{9}$Be + $^{144}$Sm, $^{168}$Er, $^{186}$W, $^{196}$Pt, $^{208}$Pb and $^{209}$Bi.

## 4 Summary

The interaction of the RIB $^{7}$Be with a $^{208}$Pb target has been studied for the first time at three near-barrier energies. The experiment benefited from the recent upgrade of the RIB In-Flight facility EXOTIC, which is now able to deliver $^{7}$Be beams energetic enough to match the energy range around the Coulomb barrier also for reactions on heavy targets. We measured the quasi-elastic scattering differential cross section and extracted the total reaction cross section. The comparison with the reaction cross sections derived for the mirror projectile $^{7}$Li and the similarly weakly-bound nucleus $^{6}$Li interacting with the same target clearly indicate that the $^{7}$Be data essentially follow the trend individuated by the heavier lithium isotopes. This outcome suggests that, for these projectiles, nuclear structure might play a more relevant role in the reaction dynamics rather then the projectile binding energy. In order to get a deeper insight on the dominant reaction mechanisms for the system $^{7}$Be + $^{208}$Pb, we started the investigation of the energy spectra and angular distributions for the inclusive production of $^{3}$He and $^{4}$He nuclei. We immediately observed that

the $^{4}$He production is a factor 4-5 higher than the $^{3}$He one, confirming that also for the interaction with heavy targets the $^{7}$Be reaction dynamics at near barrier is not dominated by the non capture breakup process. The detailed analysis of these events as well as of the coincidence events is presently in progress.

## References

[1] L.F. Canto, P.R.S. Gomes, R. Donangelo, and M.S. Hussein, Phys. Rep. **424**, 1 (2006).
[2] J.F. Liang, and C. Signorini, Int. J. Mod. Phys. E **14**, 1121 (2005).
[3] N. Keeley, R. Raabe, N. Alamanos, and J.L. Sida, Prog. Part. Nucl. Phys. **59**, 579 (2007).
[4] N. Keeley, N. Alamanos, K.W. Kemper, and K.Rusek, Prog. Part. Nucl. Phys. **63**, 396 (2009).
[5] M. Mazzocco, Int. J. Mod. Phys. E **19**, 977 (2010).
[6] N. Keeley, K.W. Kemper and K. Rusek, Eur. Phys. J. A **50**, 145 (2014).
[7] L.F. Canto, P.R.S. Gomes, R. Donangelo, J. Lubian, and M.S. Hussein, Phys. Rep. **596**, 1 (2015).
[8] M. Dasgupta *et al.*, Phys. Rev. C **70**, 024606 (2004).
[9] A. Di Pietro *et al.*, Phys. Rev. C **69**, 044613 (2004).
[10] A. Navin *et al.*, Phys. Rev. C **70**, 044601 (2004).
[11] R. Raabe *et al.*, Nature **431**, 823 (2004).
[12] A. Lemasson *et al.*, Phys. Rev. Lett. **103**, 232701 (2009).
[13] A. Lemasson *et al.*, Phys. Rev. C **82**, 044617 (2010).
[14] M. Cubero *et al.*, Phys. Rev. Lett. **109**, 262701 (2012).
[15] J.P. Fernandez-Garcia *et al.*, Phys. Rev. Lett. **110**, 142701 (2013).
[16] A. Di Pietro *et al.*, Phys. Rev. Lett. **105**, 022701 (2010)
[17] E.F. Aguilera *et al.*, Phys. Rev. C. **79**, 021601(R) (2009).
[18] E.F. Aguilera *et al.*, Phys. Rev. Lett. **107**, 092701 (2011).
[19] R. Rafiei *et al.*, Phys. Rev. C **81**, 024601 (2010).
[20] D.H. Luong *et al.*, Phys. Rev. C **88**, 034609 (2013).
[21] E.C. Simpson *et al.*, Phys. Rev. C **93**, 024605 (2016).
[22] S. Kalkal *et al.*, Phys. Rev. C **93**, 044605 (2016).
[23] K.J. Cook *et al.*, Phys. Rev. C **93**, 064604 (2016).
[24] V.Z. Maidikov *et al.*, Nucl. Phys. A **746**, 389c (2004).
[25] F. Farinon *et al.*, Nucl. Instrum. Methods B **266**, 4097 (2008).
[26] M. Mazzocco *et al.*, Nucl. Instrum. Methods B **266**, 4665 (2008).
[27] M. Mazzocco *et al.*, Phys. Rev. C. **92**, 024615 (2015).
[28] M. Mazzocco *et al.*, Nucl. Instrum. Methods B **317**, 223 (2013).
[29] E. Strano *et al.*, Nucl. Instrum. Methods B **317**, 657 (2013).
[30] D. Pierroutsakou *et al.*, Nucl. Instrum. Methods A **834**, 46 (2016).
[31] I.J. Thompson, Comput. Phys. Rep. **2**, 167 (1988).
[32] R. Broglia and A. Winther, Heavy Ion Reactions (Addison-Wesley, Reading, MA, 1990), p. 113.
[33] N. Keeley *et al.*, Nucl. Phys. A **571** (1994) 326.
[34] P.R.S. Gomes, J. Lubian, I. Padron, R.M. Anjos, Phys. Rev. C **71** (2005) 017601.
[35] A. Gavron, Phys. Rev. C **21**, 230 (1980).
[36] J. Lei and A.M. Moro, Phys. Rev. C **95**, 044605 (2017).